IEEE Access
Multidisciplinary | Rapid Review | Open Access Journal

Received 8 July 2022, accepted 27 July 2022, date of publication 1 August 2022, date of current version 4 August 2022.
Digital Object Identifier 10.1109/ACCESS.2022.3195541

RESEARCH ARTICLE

Low-Profile Six-Port Circular Patch Antenna With Six Triple-Shorted Dual-Resonant 60°-Disk Sectors to Generate Six Uncorrelated Waves for Wideband Mobile MIMO Antennas

KIN-LU WONG[1], (Fellow, IEEE), CHI-JUI HO[1], (Student Member, IEEE), AND WEI-YU LI[2], (Member, IEEE)
[1]Department of Electrical Engineering, National Sun Yat-sen University, Kaohsiung 80424, Taiwan
[2]Information and Communications Research Laboratories, Industrial Technology Research Institute, Hsinchu 31057, Taiwan
Corresponding author: Kin-Lu Wong (wongkl@mail.nsysu.edu.tw)

This work was supported by the Ministry of Science and Technology, Taiwan, under Grant MOST 109-2221-E-110-059.

ABSTRACT A low-profile six-port circular patch antenna generating six uncorrelated waves in a wide band of about 5.8-7.5 GHz (based on 3:1 VSWR, fractional bandwidth about 25%) is presented. The antenna thickness is 1.4 mm (about 0.027λ at 5.8 GHz), which includes a 0.4 mm thick FR4 substrate with the circular patch printed thereon and an additional 1.0 mm thick air layer to achieve a low-permittivity antenna substrate. The circular patch with a diameter of 40 mm (about 0.77λ at 5.8 GHz) is separated into six 60°-disk sectors by using three linear slots across the patch center and sequentially rotated by 60°. Each disk sector is short-circuited to the ground plane through three properly located shorting pins. It thus makes the 0.5-wavelngth and 0.25-wavelength resonant modes excited at nearby frequencies to form a dual-resonant wide band for each port. Additionally, the six ports in the proposed antenna have their port isolation larger than 10 dB and the corresponding six radiating waves have very low envelope correlation coefficients (less than about 0.02) over the wide band. That is, six uncorrelated waves suitable for MIMO (multi-input-multi-output) operation are obtained. The proposed antenna can find applications for wideband mobile MIMO antennas to cover 6.425-7.125 GHz of the possible new mobile communication band or 5.925-7.125 GHz for the new unlicensed WiFi-6E band.

INDEX TERMS Mobile antennas, mobile MIMO antennas, six-port single-patch MIMO antennas, low-profile six-port patch antennas.

I. INTRODUCTION

For beyond fifth-generation (5G) communication or future six-generation (6G) communication, the multi-input-multi-output (MIMO) operation with more than four over-the-air data streams to greatly enhance the data throughput has been envisioned [1], [2]. To cope with the development trend, the employment of more compact or high-density MIMO antennas for the access points and the mobile devices becomes one of the key challenges [1]. Especially, owing to the very limited space inside the mobile devices, such as the mobile phones and the laptop computers, the compact MIMO antennas suitable for mobile device applications is even more challenging.

Recently, the four-port or six-port patch antennas based on using a single radiating patch [3]–[8] to achieve compact multi-port single-patch antennas suitable for 5G or MIMO access-point applications have been reported. In order to obtain enhanced port isolation and uncorrelated radiation for the generated multiple radiating waves, various decoupling techniques for the multiple ports collocated in a single radiating patch have been demonstrated. In [3]–[5], the multi-mode antenna design technique based on the theory of the

The associate editor coordinating the review of this manuscript and approving it for publication was Hassan Tariq Chattha.

This work is licensed under a Creative Commons Attribution-NonCommercial-NoDerivatives 4.0 License.
For more information, see https://creativecommons.org/licenses/by-nc-nd/4.0/

characteristic mode [3]–[5] has been applied, which however requires using a large-size external feed network for enhanced port isolation and will therefore lead to a lower antenna efficiency and increase the complexity of the antenna design.

In [6], [7], the decoupling technique is based on placing the shorting metal walls between the radiating patch and the ground plane, so as to obtain multiple isolated resonant quadrants in a square patch [6] or multiple isolated resonant sectors in a circular patch [7]. While in [8], the decoupling technique of applying the gap-coupled shorting posts to an annular-ring patch to obtain multiple isolated annular sectors is shown. Multiple uncorrelated waves can therefore be generated. These reported multi-port single-patch MIMO antennas, however, have a high antenna profile above the ground plane (larger than 0.1 wavelength [6]–[8] or even larger than 0.3 wavelength [3]–[5] in the operating band) for MIMO access-point applications. The high antenna profile makes the reported multi-port patch antennas [3]–[8] not suitable for MIMO mobile-device applications.

In order to be promising for mobile-device applications, the antenna thickness of the multi-port patch antenna is required to be as low as possible. Some related low-profile four-port single-patch antennas have been reported [9]–[11]. The applied decoupling technique therein is all related to using multiple shorting pins to function like shorting metal walls between the top radiating patch and the ground plane. Four isolated resonant regions can therefore be obtained to generate four uncorrelated waves for MIMO applications.

It is also noted that the antenna design in [9] cannot be mounted on a large ground plane or the chassis ground plane of the mobile device. This is because the antenna's ground plane in [9] has a same size as the top radiating patch, which can lead to a wider operating band (3:1 VSWR or −6 dB impedance matching) covering the 5G band of 3.3-4.2 GHz (fractional bandwidth 24%) and however make the fringing fields around the antenna edge or boundary much stronger. The latter causes large effects on the antenna performance when the antenna is directly placed on or in very close proximity of a large ground plane.

In [10], the low-profile four-port square-ring patch antenna is proposed for wireless local area network (WLAN) MIMO application and has a relatively narrow band of only about 4% in the 2.4 GHz band. On the other hand, the four-port patch antenna with a square patch in [11] operates in a wide band of 3.3-4.2 GHz (3:1 VSWR, fractional bandwidth 24%) for 5G MIMO application. The wideband operation for the four ports is related to the $TM_{1/2,1/2}$ mode excitation supported by the four two-edge-shorted quarter-patches formed by multiple shorting pins as metal walls in the square patch antenna [11].

Note that the reported low-profile single-patch MIMO antennas in [9]–[11] are limited in generating four uncorrelated waves. For the case of generating more than four uncorrelated waves, such as at least six uncorrelated waves, the related designs for wideband mobile MIMO antennas have not yet been reported. This may be owing to the decoupling issue associated to more collocated ports in a single patch antenna will be more complex and more challenging as well. However, it is expected that this kind of low-profile multi-port single-patch antennas can find promising applications in beyond 5G or future 6G MIMO communications with more over-the-air data streams [2].

In this study, a low-profile six-port circular patch antenna with a new decoupling and wideband technique, other than those in [3]–[11], to generate six uncorrelated waves in a wide band of about 5.8-7.5 GHz (based on 3:1 VSWR, fractional bandwidth about 25%) is presented. The proposed antenna can be applied for wideband mobile MIMO antennas to cover 6.425-7.125 GHz of the possible new mobile communication band for beyond 5G communication [12] or 5.925-7.125 MHz for the new unlicensed WiFi-6E band [13].

The proposed antenna has a low profile of 1.4 mm (about 0.027λ at 5.8 GHz) above the ground plane. To generate six uncorrelated waves, the circular patch in the proposed antenna is separated into six 60°-disk sectors by using three linear slots across the patch center and sequentially rotated by 60°. A triple-shorting technique is then applied to each disk sector to make its 0.5-wavelength and 0.25-wavelength resonant modes excited with good impedance matching and at nearby frequencies to form a dual-resonant wide band for each port.

At the same time, the port isolation of the six ports in the proposed antenna can be enhanced to be larger than 10 dB over the wide band, as good as the port isolation obtained in the low-profile four-port single-patch MIMO antennas reported in [9]–[11]. That is, the triple-shorting technique applied here can lead to both decoupling improvement and wideband operation for the proposed antenna. Six uncorrelated waves can also be obtained with very low envelope correlation coefficients (less than 0.05) over the wide band for MIMO operation. Details of the antenna structure, working principle, design considerations, and parametric study based on using the three-dimensional high frequency electromagnetic simulation software (ANSYS HFSS) [14] for the proposed antenna are presented. An experimental study of the proposed antenna is also conducted to verify the simulation results.

II. ANTENNA STRUCTURE AND PERFORMANCE

Fig. 1 shows the proposed low-profile six-port (Ports 1-6) circular patch antenna for wideband mobile MIMO antenna applications. Six 60°-disk sectors (Sectors ① -⑥) are formed in the circular patch through three linear slot (width 1 mm) across the patch center as shown in the figure. In each sector, a triple-shorting technique for decoupling improvement and wideband operation is applied (see three shorting pins of diameter 1.6 mm at S1, S2, S3 shown in Sector ①). Based on the 3:1 VSWR impedance matching for the mobile antenna design requirement [9]–[11], [15]–[18], the proposed antenna covers a wide band of about 5.8-7.5 GHz (1.7 GHz in bandwidth or about 25% in fractional bandwidth). The wideband operation for all the six ports is obtained owing to the 0.5-wavelngth and 0.25-wavelength resonant modes

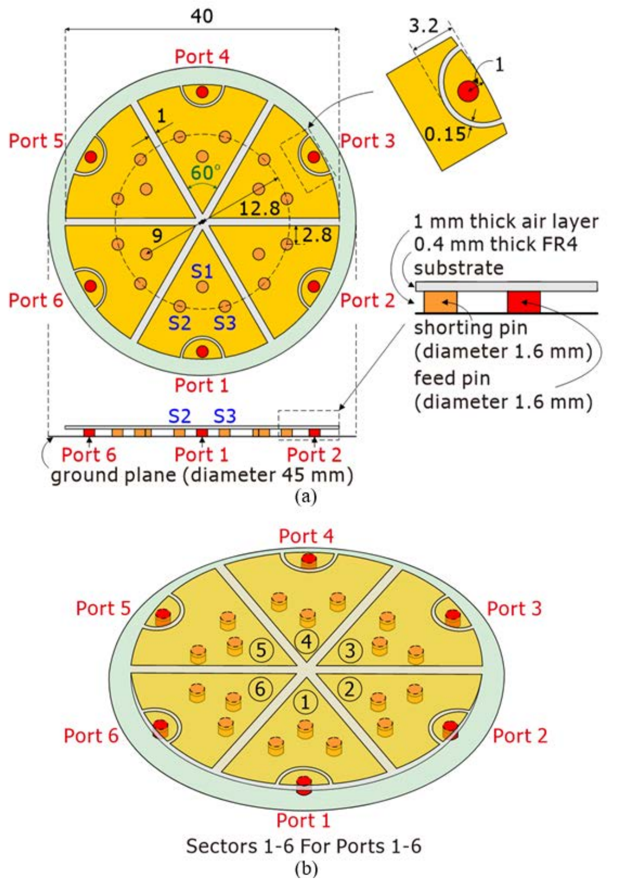

FIGURE 1. Geometry of the low-profile wideband six-port circular patch antenna. (a) Top and side views. (b) Perspective view.

being excited with good impedance matching at nearby frequencies to form a dual-resonant wide band for each port in the proposed antenna.

To support the generation of six uncorrelated waves, the circular patch in the proposed antenna has a diameter of 40 mm, about 0.77λ at 5.8 GHz (the lower-edge frequency of the wide operating band). The antenna substrate is formed by a 0.4 mm thick FR4 substrate with the circular patch printed thereon and an additional 1.0 mm thick air layer between the FR4 substrate and the ground plane. The ground plane is also selected to be in a circular shape with 45 mm in diameter.

The antenna substrate above the ground plane has a total thickness of 1.4 mm (about 0.027λ at 5.8 GHz) and has an equivalent relative permittivity of about 1.28. Note that, with a low relative permittivity close to that of air, the excited resonant modes of the shorted patch antenna, especially the 0.25-wavelength mode, can have a wider operating bandwidth [19]. Also, the operating bandwidth and antenna thickness with respect to the lowest operating wavelength of the proposed six-port patch antenna are comparable to those in the reported low-profile wideband four-port patch antennas [9], [11]. In Ref. [9], the reported 3:1 VSWR fractional bandwidth is 24% (3.3-4.2 GHz) and the antenna thickness is about 0.022λ at 3.3 GHz. In Ref. [11], the reported 3:1 VSWR

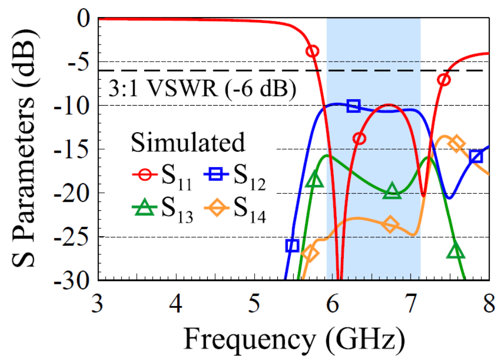

FIGURE 2. Simulated S parameters of Port 1 in the proposed antenna.

fractional bandwidth is 24% (3.3-4.2 GHz) and the antenna thickness is about 0.026λ at 3.3 GHz.

To demonstrate the antenna performance, Fig. 2 shows the simulated *S* parameters of Port 1 in the proposed antenna. The results of Ports 2-6 are same as that of Port 1, owing to the symmetric structure of Ports 1-6 in the proposed antenna. Each sector is excited by a probe feed located at the center of the sector's outer curved edge. All the six probe feeds are therefore equally spaced by 60° along the boundary of the circular patch. Each probe feed capacitively couples through a semi-circular gap of 0.15 mm to excite the corresponding sector.

Two resonant modes are seen to be excited at nearby frequencies (at about 6.1 GHz and 7.2 GHz) to form a wide band of about 5.8-7.5 GHz [based on 3:1 VSWR (-6 dB)] impedance matching for mobile antenna application. Note that the colored frequency region in the figure indicates 5.925-7.125 GHz, which covers 6.425-7.125 GHz of the possible new mobile communication band for beyond 5G communication [12] and 5.925-7.125 MHz for the new unlicensed WiFi-6E band [13].

Also, the transmission coefficients [S_{12} (= S_{16}), S_{13} = (S_{15}), S_{14}] are less than about −10 dB over the operating band, which is comparable to those of the reported low-profile wideband four-port patch antennas [9], [11]. The S_{13} and S_{14} are even less than −15 dB for almost all frequencies in the operating band.

The simulated antenna efficiency of Port 1 in the proposed antenna is shown in Fig. 3. The antenna efficiency shown in the figure includes the mismatching losses. The antenna efficiency is about 57%-63% over the operating band. Fig. 4 shows the simulated envelope correlation coefficients (ECC_{ij}) for two ports (Ports *i* and *j*) in the proposed antenna. The simulated ECCs [ECC_{12} (= ECC_{16}), ECC_{13} (= ECC_{15}), ECC_{14}] are less than about 0.02 over the operating band. Note that the simulated ECCs are obtained from simulation software HFSS [14] by applying the expression based on the three-dimensional radiated electric fields [20], [21]. The obtained low ECC values suggest that the six radiated waves can be considered to be generally uncorrelated and suitable for MIMO applications.

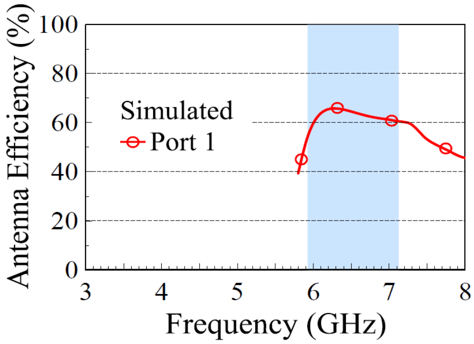

FIGURE 3. Simulated antenna efficiency of Port 1 in the proposed antenna.

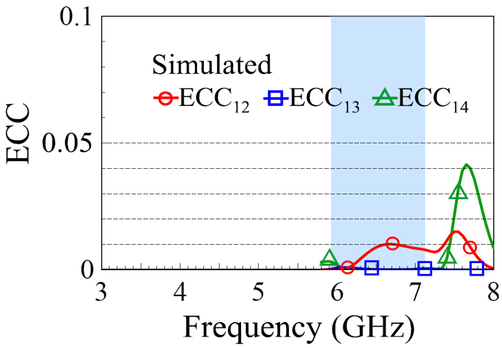

FIGURE 4. Simulated envelope correlation coefficients (ECC_{ij}) for two ports (Ports *i* and *j*) in the proposed antenna.

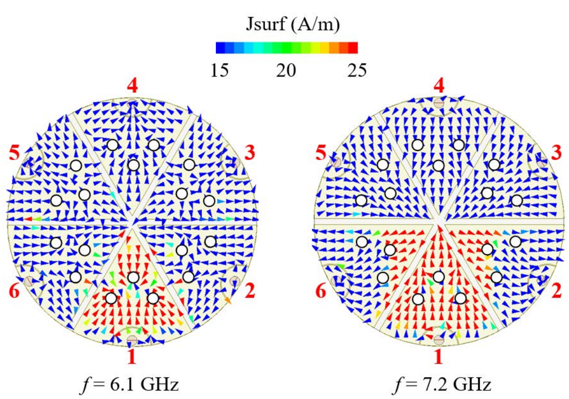

FIGURE 5. Simulated vector surface current distributions at 6.1 GHz and 7.2 GHz of Port 1 excited in the proposed antenna.

Fig. 5 shows the simulated vector surface current distributions at 6.1 GHz and 7.2 GHz of Port 1 excited in the proposed antenna. Strong surface currents are seen to be generally confined inside Sector ① for Port 1 excitation, especially at 6.1 GHz. At 7.2 GHz, some surface currents coupled from Sector ① to its two adjacent sectors (Sectors ② and ⑥) are mainly confined between the triple shorting positions and the patch center, away from Ports 2 and 6. Also, relatively very weak surface currents are seen in Sectors ③, ④, and ⑤. The results conform to the transmission coefficients observed in Fig. 2.

In addition, the surface currents at 7.2 GHz are seen to be directed from Port 1 to the patch center, which indicates that the 0.5-wavelength mode of Sector ① is excited. On the other hand, the surface currents at 6.1 GHz are directed toward triple shorting positions at S1, S2 and S3. This indicates that the 0.25-wavelength mode is excited, which however is modified by the additional shorting pins at S2 and S3 to the shorting pin at S1. That is, the excited 0.25-wavelength and 0.5-wavelength modes accounts for the dual-resonant wide band obtained in the proposed antenna.

III. WORKING PRINCIPLE AND DESIGN CONSIDERATIONS

With the aid of Cases A, B, and C shown in Fig. 6, the working principle and design considerations for the decoupling improvement and wideband operation of the proposed antenna are further analyzed. Case A in Fig. 6(a) is the case without shorting pins in each sector and Case B in Fig. 6(b) is the case with one shorting pin S1 along the centerline of each sector, with a distance of 9.5 mm to the patch center.

Case C in Fig. 6(c) is the case with two shorting pins in each sector, with the first shorting pin S1 same as in Case B and the second shorting pin S2 placed at 12.8 mm to the patch center and 2.8 mm to the linear slot separating two adjacent sectors. Corresponding dimensions of Cases A to C are same as those shown in Fig. 1 for the proposed antenna. The three cases can be considered as three design steps to obtain the proposed antenna.

Fig. 7 shows the simulated *S* parameters of Port 1 for Cases A to C. Their corresponding simulated vector surface current distributions of Port 1 are presented in Fig. 8. When there are no shorting pins added in each sector, a resonant mode is seen to be excited at about 6.5 GHz [see the result of Case A in Fig. 7(a)]. Its surface currents on the circular patch shown in Fig. 8(a) are also very similar as that of 7.2 GHz in Fig. 5. That is, a 0.5-wavelength mode is excited for each sector in Case A.

It is also noted that the centerline of each sector is about 19.5 mm (about 0.42λ at 6.5 GHz), the 0.5-wavelength mode can therefore be supported. However, the transmission coefficient (S_{12}) of two adjacent sectors reaches about −7 dB. Therefore, in addition to the narrow bandwidth for Case A, its port isolation between two adjacent sectors needs to be improved.

For Case B, with the adding of the shorting pin S1, two resonant modes are excited at about 3.5 GHz and 7.0 GHz as shown in Fig. 7(b). Their corresponding surface currents on the circular patch are given in Fig. 8(b). The one at about 7.0 GHz is the 0.5-wavelength mode, which is slightly shifted from about 6.5 GHz in Case A to higher frequencies owing to the shorting pin S1. On the other hand, the one at 3.5 GHz is the 0.25-wavelength mode, whose surface currents are directed toward the shorting pin S1, which short-circuits the circular patch to the ground plane.

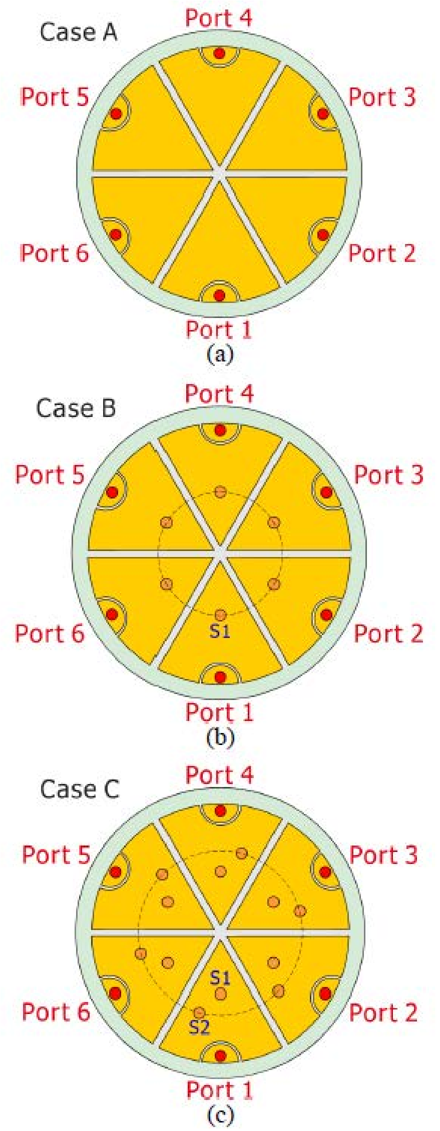

FIGURE 6. **Geometries of (a) the case without shorting pins in each sector (Case A), (b) the case with one shorting pin S1 in each sector (Case B), and (c) the case with two shorting pins (S1, S2) in each sector (Case C). Corresponding dimensions are same as the proposed antenna in Fig. 1.**

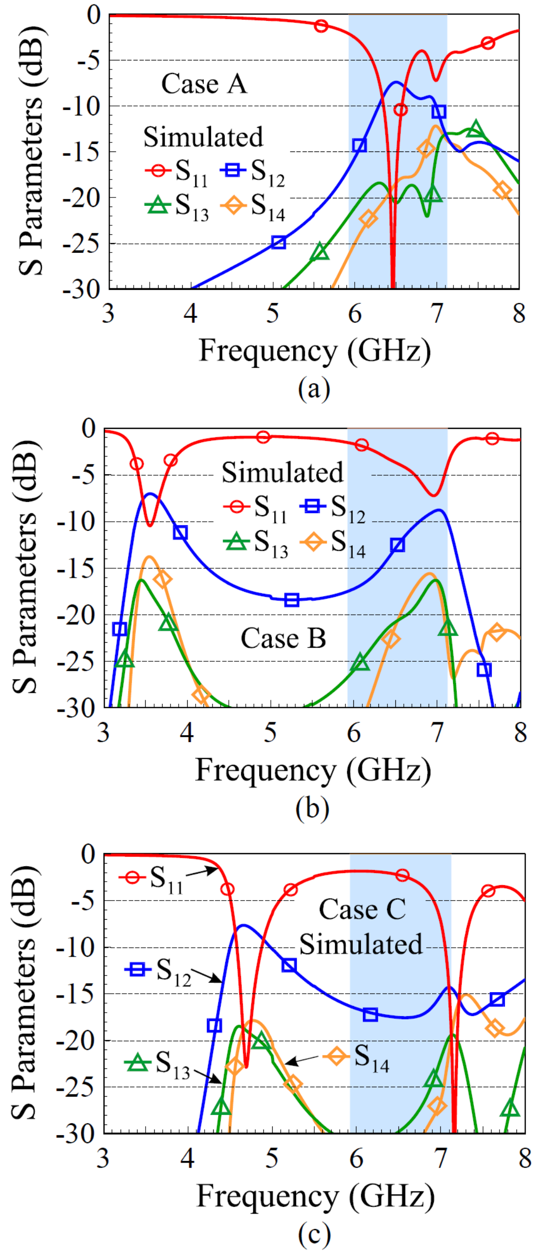

FIGURE 7. **Simulated S parameters of Port 1. (a) Case A. (b) Case B. (c) Case C.**

However, the S_{12} between two adjacent sectors for the two resonant modes is still large in Case B, especially that at 3.5 GHz is about −7 dB. That is, although two resonant modes are generated, they are still widely separated and wideband operation cannot be obtained. The port isolation between two adjacent sectors also needs to be improved.

For Case C, two resonant modes at about 4.7 GHz and 7.2 GHz are excited as seen in Fig. 7(c) and their corresponding surface currents are shown in Fig. 8(c). Note that, owing to the additional shorting pin S2 added in each sector, the effective resonant length of the 0.25-wavelength mode is decreased, which causes the 0.25-wavelength mode shifted from about 3.5 GHz in Case B to about 4.7 GHz in Case C.

The 0.5-wavelength mode is also slightly shifted from about 7.0 GHz in Case B to about 7.2 GHz in Case C. In addition, the S_{12} between two adjacent sectors is decreased, which is because the second shorting pin S2 is placed closer to one adjacent sector in Case C. This can decrease the surface currents near one radial boundary of the excited sector from entering into its one adjacent sector, thereby improving the port isolation between two adjacent sectors.

By further adding a third shorting pin S3 to each sector in Case C, the effective resonant length of the 0.25-wavelength can be further decreased and the surface currents near two radial boundaries of the excited sector entering into its two adjacent sectors can also be decreased. Therefore, as discussed for the results shown in Fig. 2 for the proposed antenna, two resonant modes (0.25-wavelength and

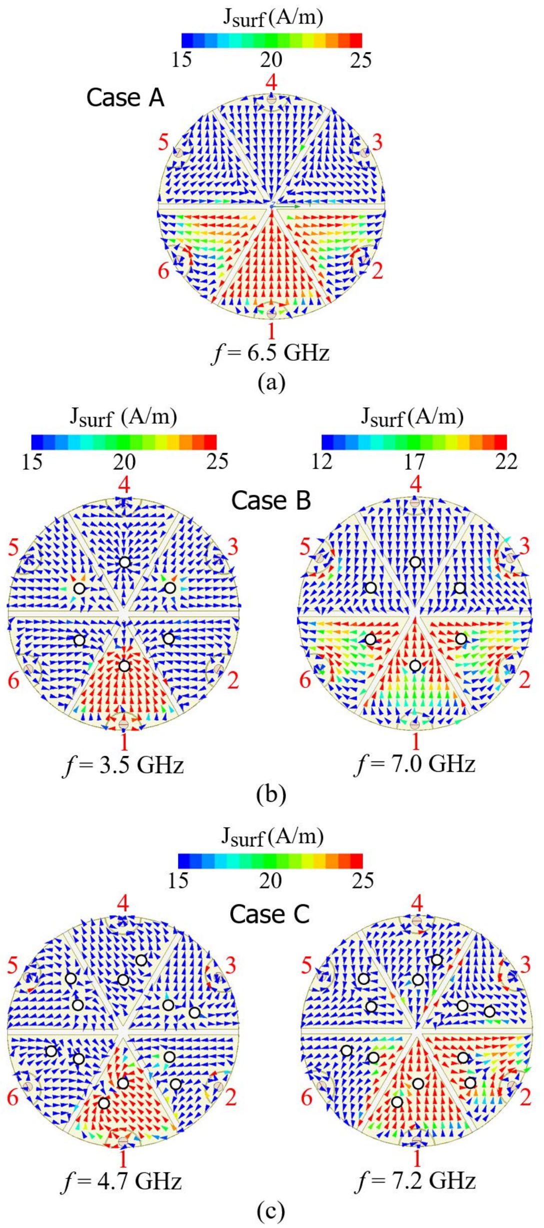

FIGURE 8. Simulated vector surface current distributions of Port 1 excited with other ports terminated to 50 Ω. (a) Case A. (b) Case B. (c) Case C.

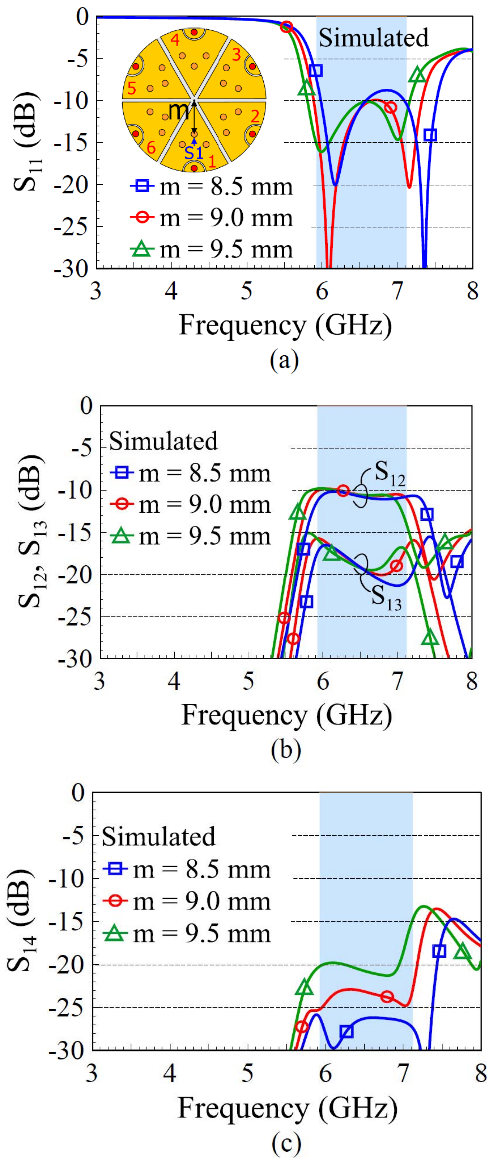

FIGURE 9. Simulated *S* parameters of Port 1 for different positions (*m*) of the shorting pin S1 along the centerline of each sector. (a) S_{11}. (b) S_{12}, S_{13}. (c) S_{14}.

0.5-wavelength modes) are excited at closer frequencies at 6.1 and 7.2 GHz to obtain a dual-resonant wide band. Also, the S_{12} between two adjacent sectors is further decreased [see the results in Fig. 8(c) for Case C vs. Fig. 2 for the proposed antenna]. That is, the triple-shorting technique applied in the proposed antenna leads to decoupling improvement and wideband operation of the six ports.

IV. PARAMETRIC STUDY

A parametric study of typical design parameters to finely adjust the antenna performance is also conducted. Effects of varying the positions of the shorting pins S1, S2, and S3 are studied in Figs. 9 and 10. Results of varying the slot width to form Sectors ①-⑥ in the proposed antenna are presented in Fig. 11. Varying the coupling gap at Ports 1-6 to adjust the antenna's impedance matching is shown in Fig. 12. Effects of the ground plane size are also analyzed in Fig. 13.

Fig. 9 shows the simulated *S* parameters of Port 1 for different positions of the shorting pin S1 along the centerline of each sector in the proposed antenna. Other dimensions are fixed as shown in Fig. 1. Results for the S1 position (*m*) varied from 8.5 mm to 9.5 mm are presented.

It is seen in Fig. 9(a) that the resonant frequencies of the lower mode (0.25-wavelength mode) and the upper mode (0.5-wavelength mode) are slightly varied and their formed wide operating band can still cover 5.925-7.125 GHz (the colored frequency region). The impedance matching of the

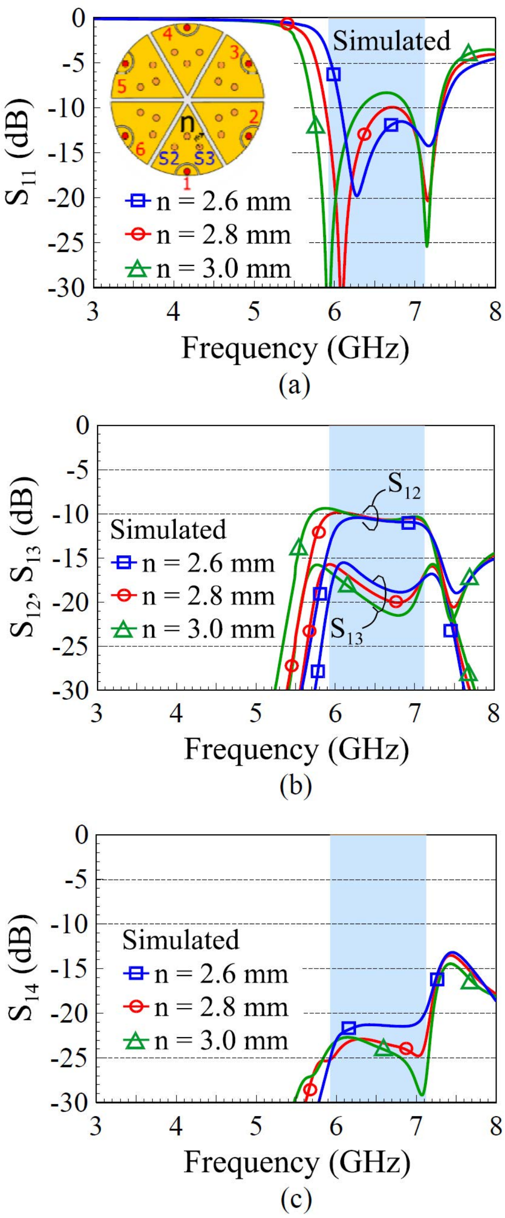

FIGURE 10. Simulated *S* parameters of Port 1 for the shorting pins S2 and S3 with various distances (*n*) to the adjacent sectors. (a) S_{11}. (b) S_{12}, S_{13}. (c) S_{14}.

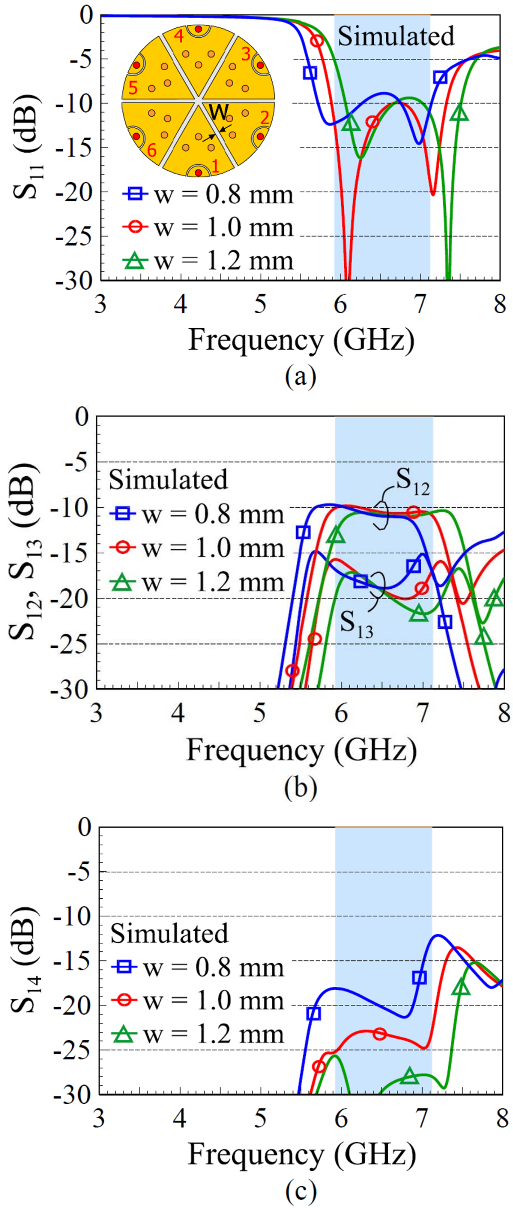

FIGURE 11. Simulated *S* parameters of Port 1 for different slot widths (*w*) to form six 60°-disk sectors. (a) $S11$. (b) S_{12}, S_{13}. (c) S_{14}.

two modes, however, can be effectively varied. This provides as a means to finely adjust the impedance matching of the antenna's wide operating band.

For the S_{12} and S_{13} shown in Fig. 9(b), small variations are seen. Also, the S_{14} shown in Fig. 9(c) is still better than the S_{12} and S_{13}. The results indicate that the impedance matching over the antenna's wide operating band can be finely adjusted by varying the S1 position, with no significant variations in the port isolation.

Fig. 10 shows the simulated *S* parameters of Port 1 for the shorting pins S2 and S3 with various distances to the adjacent sectors. The distance *n* in the figure is the length between the slot edge and the center of the shorting pin S2 or S3 (copper post of diameter 1.6 mm). Results of the distance *n* varied from 2.6 mm to 3.0 mm are presented. Relatively larger effects on the resonant frequency of the 0.25-wavelength mode than that of the 0.5-wavelength mode are seen in Fig. 10(a). That is, by finely adjusting the distance *n* of the shorting pins S2 and S3, the 0.25-wavelength mode can be adjusted to occur at a proper frequency to the 0.5-wavelength mode, thereby forming a wide operating band for the proposed antenna. In addition, the effects on the port isolation are relatively small as seen in Fig. 10(b) and (c).

Fig. 11 shows the simulated *S* parameters of Port 1 for different slot widths (*w*) to form six 60°-disk sectors. Since a larger slot width will decrease the effective resonant area of each sector, both the excited 0.25-wavelength and

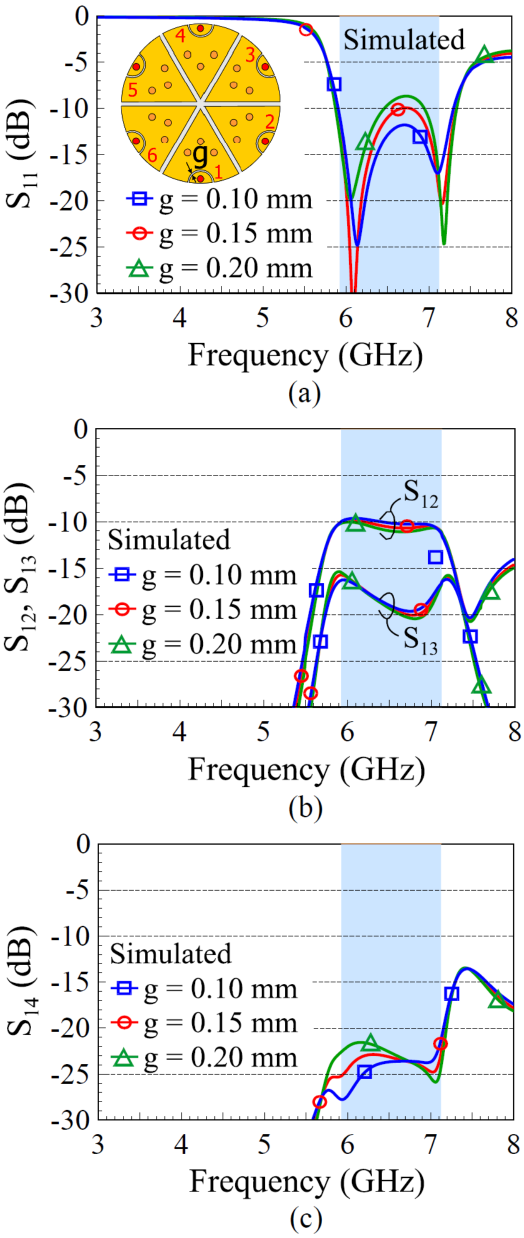

FIGURE 12. Simulated S parameters of Port 1 for different coupling gaps (g) at the feed port. (a) S_{11}. (b) S_{12}, S_{13}. (c) S_{14}.

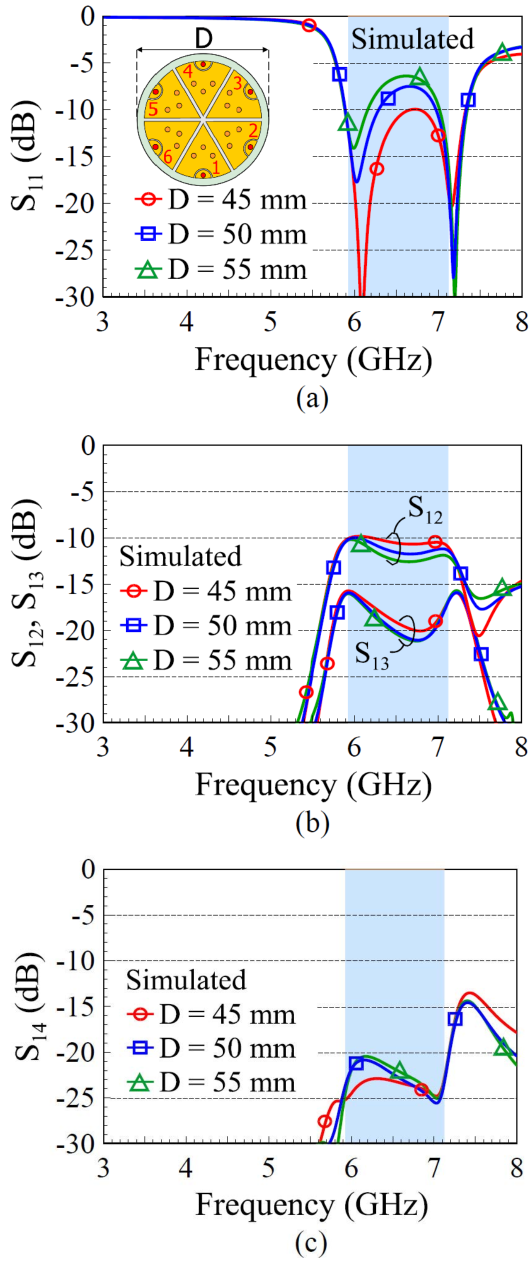

FIGURE 13. Simulated S parameters of Port 1 for different diameters (D) of the ground plane. (a) S_{11}. (b) S_{12}, S_{13}. (c) S_{14}.

0.5-wavelength modes are seen to occur at higher frequencies for the slot width varied from 0.8 mm to 1.2 mm [see Fig. 11(a)]. At the same time, the transmission coefficients (S_{12}, S_{13}, S_{14}) over the wide operating band can still be less than about 10 dB as seen in Fig. 11(b) and (c).

The simulated S parameters of Port 1 for the coupling gap (g) varied from 0.1 mm to 0.2 mm are presented in Fig. 12. The results indicate that adjusting the coupling gap can finely adjust the S_{11} over the wide operating band [see Fig. 12(a)], with very small effects on the transmission coefficients of the S_{12}, S_{13}, and S_{14} as seen in Fig. 12(b) and (c).

Fig. 13 shows the simulated S parameters of Port 1 for different diameters (D) of the ground plane. With the antenna dimensions fixed, the results for the ground diameter varied from 45 mm to 55 mm are presented. The two resonant modes are seen to occur at about the same frequencies and their impedance matching are still less than −6 dB over the antenna's wide operating band [see the S_{11} in Fig. 13(a)]. Small effects on the transmission coefficients S_{12}, S_{13}, and S_{14} are also seen in Fig. 13(b) and (c). Based on the obtained results, the typical design parameters studied in Figs. 9-13 can be applied in finely adjusting the performance of the proposed antenna.

V. EXPERIMENTAL RESULTS AND DISCUSSION

The proposed six-port patch antenna was fabricated as shown in Fig. 14 and tested to verify the simulation results. The

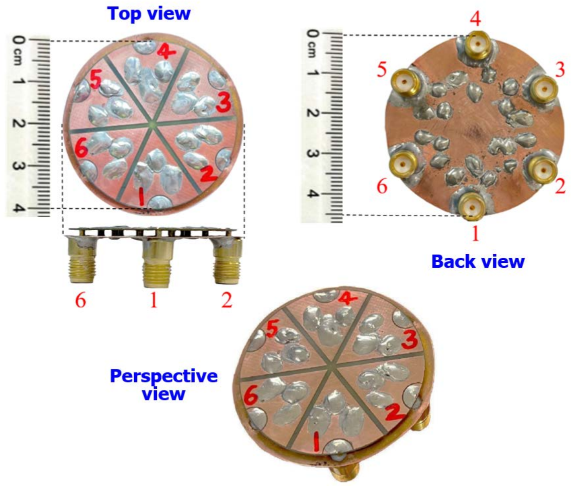

FIGURE 14. Fabricated six-port patch antenna.

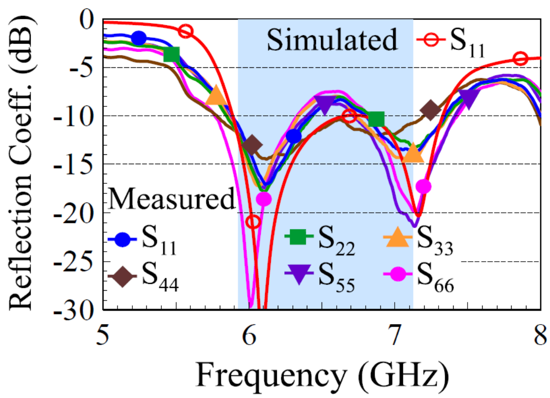

FIGURE 15. Measured reflection coefficients of the fabricated antenna.

measured reflection coefficients for Ports 1-6 are shown in Fig. 15. The simulated S_{11} (= S_{ii}, i = 2-6) is included in the figure for comparison, and agreement between the measured and simulated results is observed. The fabricated prototype shows a wide operating band as indicated in the simulation study.

The measured transmission coefficients of S_{12}, S_{23}, S_{34}, S_{45}, S_{56} for two adjacent ports are presented in Fig. 16(a). Those of S_{13}, S_{24}, S_{35}, S_{46} for two ports spaced by a 60°-disk sector are shown in Fig. 16(b), and those of S_{14}, S_{25}, S_{36} for two ports spaced by two 60°-disk sectors are shown in Fig. 16(c). The measured data are seen to generally agree with the corresponding simulated results shown in the figure for comparison. For the application in 5.925-7.125 GHz band (the colored frequency region in the figure), the measured isolation for two adjacent ports is larger than 10 dB as seen in Fig. 16(a). Moreover, the measured isolation for two ports spaced by one sector and two sectors is respectively larger than 15 dB in Fig. 16(b) and 20 dB in Fig. 16(c).

The antenna's radiation performance was measured in a far-field anechoic chamber and the measured results are obtained by calibrating with respect to a standard horn antenna. Fig. 17 shows the measured antenna efficiency of Ports 1-6 of the fabricated antenna. Measured results show

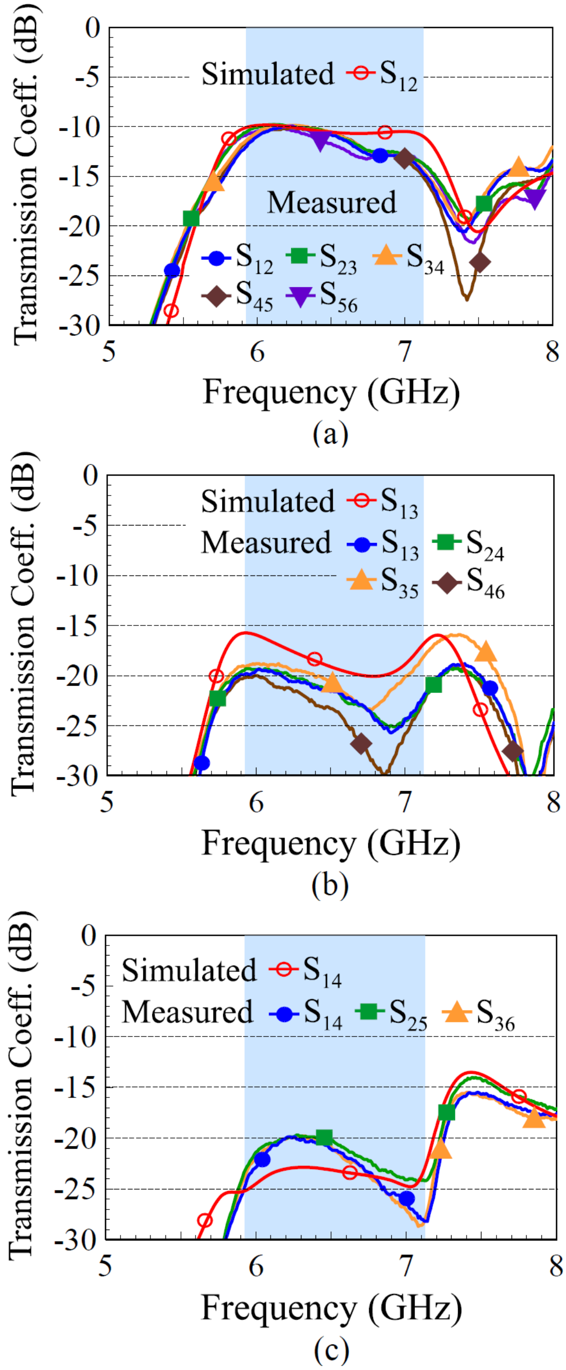

FIGURE 16. Measured transmission coefficients of the fabricated antenna. (a) S_{12}, S_{23}, S_{34}, S_{45}, S_{56}. (b) S_{13}, S_{24}, S_{35}, S_{46}. (c) S_{14}, S_{25}, S_{36}.

agreement with the simulated results shown in the figure for comparison. The measured antenna efficiency is about 50%-62% over the operating band.

The measured and simulated normalized radiation patterns at 6.1 GHz and 7.2 GHz for Port 1 in the $\phi = 0°$ plane, Port 2 in the $\phi = 60°$ plane, and Port 3 in the $\phi = 120°$ plane are respectively plotted in Fig. 18(a), (b), and (c). That is, the radiation patterns in the plane along the centerline of each sector are plotted. The corresponding radiation patterns for Port 4 in the $\phi = 180°$ plane, Port 5 in the $\phi = 240°$

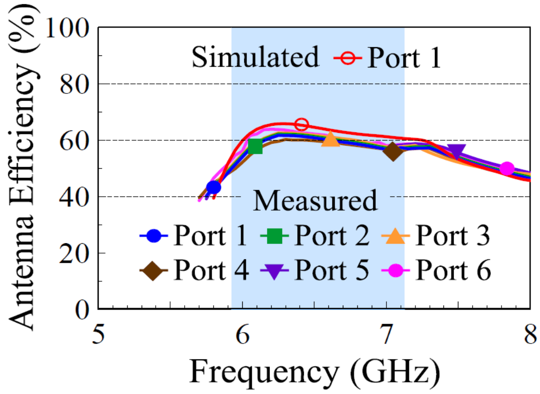

FIGURE 17. Measured antenna efficiency of the fabricated antenna.

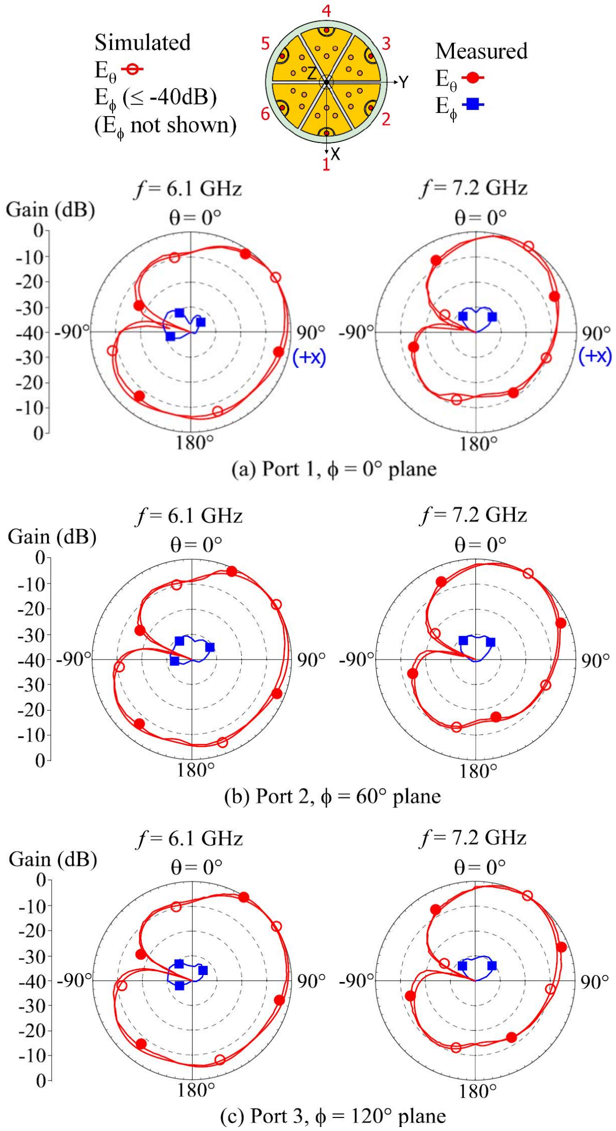

FIGURE 18. Measured and simulated normalized radiation patterns at 6.1 GHz and 7.2 GHz for the fabricated antenna. (a) Port 1, $\varphi = 0°$ plane. (b) Port 2, $\varphi = 60°$ plane. (c) Port 3, $\varphi = 120°$ plane.

plane, and Port 6 in the $\phi = 300°$ plane are shown in Fig. 19(a), (b), and (c). Note that the simulated E_ϕ radiation is very small, less than −40 dB, in the radiation pattern along the

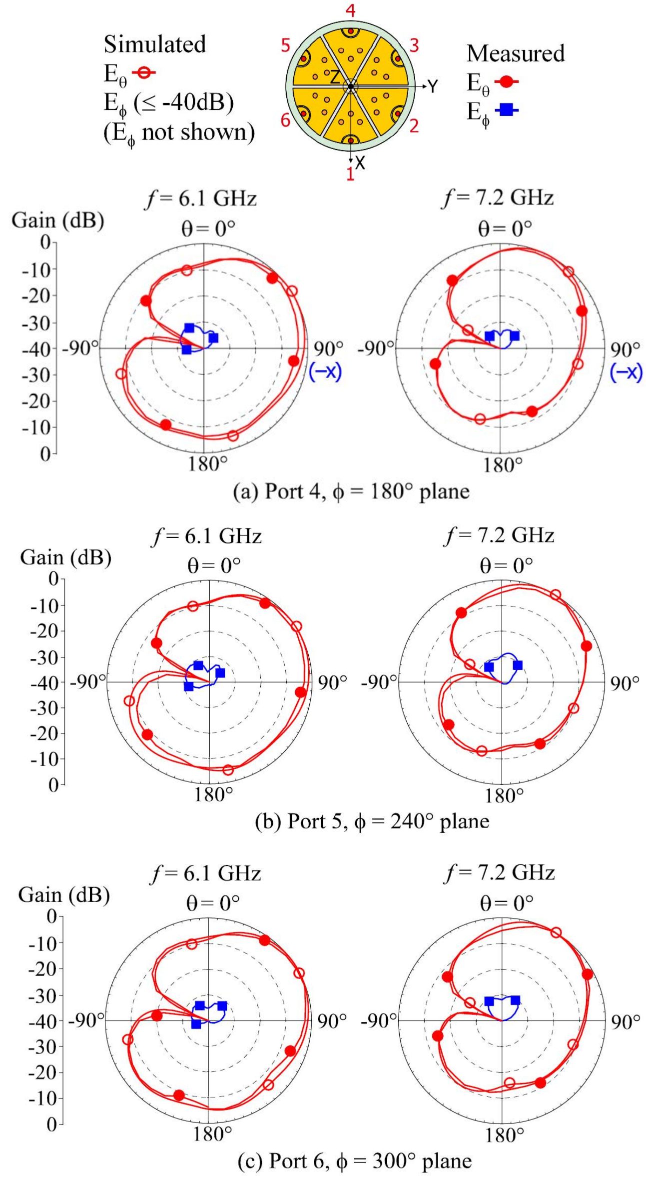

FIGURE 19. Measured and simulated normalized radiation patterns at 6.1 GHz and 7.2 GHz for the fabricated antenna. (a) Port 4, $\varphi = 180°$ plane. (b) Port 5, $\varphi = 240°$ plane. (c) Port 6, $\varphi = 300°$ plane.

centerline of each resonant sector. The simulated E_φ radiation is therefore not shown in the figure. For the E_θ radiation, good agreement between the measured and simulated results is observed.

Also, the radiation patterns for each sector are seen to be tilted away from the z-direction ($\theta = 0°$) toward the feed port. For example, for Ports 1 and 4, their radiation patterns are tilted toward $+x$ direction and $-x$ direction, respectively. This is mainly because the excited surface currents are stronger near the feed located at the curved patch edge. This behavior may also help to achieve very low envelope correlation coefficients (ECCs) as shown in Fig. 20, in which the ECCs are calculated based on using the measured three-dimensional (3-D) radiation patterns [20], [21]. The amplitude and phase of the measured electric fields in the 3-D radiation patterns are applied in the radiation-based ECC equation in [20].

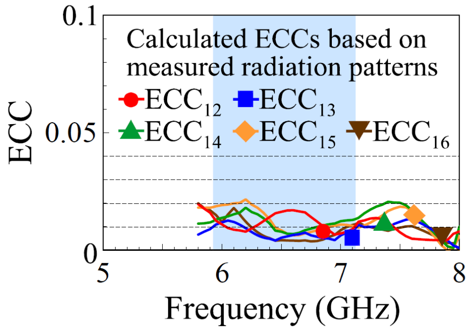

FIGURE 20. Calculated ECCs based on measured three-dimensional radiation patterns.

In Fig. 20, the ECCij is the envelope correlation coefficient between the radiating waves excited by Ports *i* and *j*. The obtained ECCs are seen to be less than about 0.02 over the wide operating band, which is similar to the simulated ECCs obtained based on using the simulated radiation patterns shown in Fig. 4. Since very low ECCs are obtained, the proposed antenna can be considered to generate six uncorrelated waves. This will be attractive for practical mobile MIMO antenna applications.

VI. CONCLUSION

A low-profile six-port circular patch antenna with six 60°-disk sectors to generate six uncorrelated waves for wideband mobile MIMO antenna has been proposed. A triple-shorting technique is applied in each sector of the proposed antenna to excite the 0.25-wavelength and 0.5-wavelength resonant modes of the 60°-disk sector to achieve dual-resonant wideband operation and port isolation improvement. The wide operating band of about 5.8-7.5 GHz is obtained, with a low profile antenna structure (antenna thickness 1.4 mm, about 0.027λ at 5.8 GHz). The isolation of any two ports over the wide band is larger than 10 dB, and those of two non-adjacent ports can even be better than 15 dB for almost all frequencies over the wide band. The measured antenna efficiency of about 50%-62% has also been obtained for Ports 1-6 in the proposed antenna. Very low envelope correlation coefficients (less than about 0.02) of the six generated waves have also been observed. Promising applications of the proposed antenna for wideband mobile MIMO antennas to cover 6.425-7.125 GHz or 5.925-7.125 GHz for the possible new mobile communication band [12] or the new unlicensed WiFi-6E band [13] are expected.

REFERENCES

[1] (Jan. 7, 2022). *MediaTek 6G Vision Whitepaper*. [Online]. Available: https://www.mediatek.com/whitepapers/6g

[2] K.-L. Wong, "5G/B5G multi-Gbps antennas for user terminals and their throughput verification," in *Proc. IEEE Asia–Pacific Microw. Conf. (APMC)*, Dec. 2020, pp. 366–368.

[3] W. Su, Q. Zhang, S. Alkaraki, Y. Zhang, X.-Y. Zhang, and Y. Gao, "Radiation energy and mutual coupling evaluation for multimode MIMO antenna based on the theory of characteristic mode," *IEEE Trans. Antennas Propag.*, vol. 67, no. 1, pp. 74–84, Jan. 2019.

[4] N. L. Johannsen, N. Peitzmeier, P. A. Hoeher, and D. Manteuffel, "On the feasibility of multi-mode antennas in UWB and IoT applications below 10 GHz," *IEEE Commun. Mag.*, vol. 58, no. 3, pp. 69–75, Mar. 2020.

[5] N. Peitzmeier, T. Hahn, and D. Manteuffel, "Systematic design of multimode antennas for MIMO applications by leveraging symmetry," *IEEE Trans. Antennas Propag.*, vol. 70, no. 1, pp. 145–155, Jan. 2022.

[6] K.-L. Wong, X.-Q. Ye, and W.-Y. Li, "Wideband four-port single-patch antenna based on the quasi-TM1/2,1/2 mode for 5G MIMO access-point application," *IEEE Access*, vol. 10, pp. 9232–9240, 2022.

[7] K.-L. Wong, Z.-W. Tso, and W.-Y. Li, "Very-wide-band six-port single-patch antenna with six uncorrelated waves for MIMO access points," *IEEE Access*, vol. 10, pp. 69555–69567, 2022.

[8] K.-L. Wong, J.-Z. Chen, and W.-Y. Li, "Four-port wideband annular-ring patch antenna generating four decoupled waves for 5G multi-input–multi-output access points," *IEEE Trans. Antennas Propag.*, vol. 69, no. 5, pp. 2946–2951, May 2021.

[9] L. Chang and H. Wang, "Miniaturized wideband four-antenna module based on dual-mode PIFA for 5G 4 × 4 MIMO applications," *IEEE Trans. Antennas Propag.*, vol. 69, no. 9, pp. 5297–5304, Sep. 2021.

[10] K.-L. Wong, C.-J. Chen, and W.-Y. Li, "Integrated four low-profile shorted patch dual-band WLAN MIMO antennas for mobile device applications," *IEEE Trans. Antennas Propag.*, vol. 69, no. 6, pp. 3566–3571, Jun. 2021.

[11] K. L. Wong, M. F. Jian, and W. Y. Li, "Low-profile wideband four-corner-fed square patch antenna for 5G MIMO mobile antenna application," *IEEE Antennas Wireless Propag. Lett.*, vol. 20, no. 12, pp. 2054–2058, Dec. 2021.

[12] (Nov. 6, 2019). *WRC-19 (World Radiocommunication Conference 2019) Report. Key Outcomes of the WRC-19*. [Online]. Available: https://www.itu.int/en/itunews/Documents/2019/2019-06/2019_ITUNews06-en.pdf

[13] (Apr. 2, 2020). *Unlicensed Use of the 6 GHz Band*. Federal Communications Commission Fact Sheet. [Online]. Available: https://docs.fcc.gov/public/attachments/DOC-363490A1.pdf

[14] (Mar. 1, 2022). *3D High Frequency Electromagnetic Simulation Software, ANSYS HFSS*. [Online]. Available: https://www.ansys.com/products/electronics/ansys-hfss

[15] S.-C. Chen, J.-L. Zhu, and C.-I.-G. Hsu, "Compact double shorted loop sub-6-GHz dual-band MIMO quad-antenna system," *IEEE Access*, vol. 9, pp. 114672–114679, 2021.

[16] I. R. R. Barani, K.-L. Wong, Y.-X. Zhang, and W.-Y. Li, "Low-profile wideband conjoined open-slot antennas fed by grounded coplanar waveguides for 4 × 45 G MIMO operation," *IEEE Trans. Antennas Propag.*, vol. 68, no. 4, pp. 2646–2657, Apr. 2020.

[17] M.-Y. Li, Y.-L. Ban, Z.-Q. Xu, J. Guo, and Z.-F. Yu, "Tri-polarized 12-antenna MIMO array for future 5G smartphone applications," *IEEE Access*, vol. 6, pp. 6160–6170, 2017.

[18] Y.-L. Ban, C. Li, C.-Y.-D. Sim, G. Wu, and K.-L. Wong, "4G/5G multiple antennas for future multi-mode smartphone applications," *IEEE Access*, vol. 4, pp. 2981–2988, 2016.

[19] K. F. Lee, Y. X. Guo, J. A. Hawkins, R. Chair, and K. M. Luk, "Theory and experiment on microstrip patch antennas with shorting walls," *IEE Proc.–Microw., Antennas Propag.*, vol. 147, no. 6, pp. 521–525, Dec. 2000.

[20] A. Iqbal, A. Altaf, M. Abdullah, and M. Alibakhshikenar, "Modified U-shaped resonator as decoupling structure in MIMO antenna," *Electronics*, vol. 9, no. 8, p. 1321, 2020.

[21] S. Blanch, J. Romeu, and I. Coebella, "Exact representative of antenna system diversity performance from input parameter description," *Electron. Lett.*, vol. 39, pp. 705–707, May 2003.

KIN-LU WONG (Fellow, IEEE) received the B.S. degree in electrical engineering from the National Taiwan University, Taipei, Taiwan, in 1981, and the M.S. and Ph.D. degrees in electrical engineering from Texas Tech University, Lubbock, TX, USA, in 1984 and 1986, respectively.

From 1986 to 1987, he was a Visiting Scientist with the Max-Planck-Institute for Plasma Physics, Munich, Germany. Since 1987, he has been with the Electrical Engineering Department, National Sun Yat-sen University (NSYSU), Kaohsiung, Taiwan, where he became a Professor, in 1991. From 1998 to 1999, he was a Visiting Scholar with the Electro Science Laboratory, The Ohio State University, Columbus, OH, USA. He was elected to be a Sun Yat-sen Chair Professor at NSYSU, in 2005, a Distinguished Chair Professor at NSYSU, in 2017, and the National Chair Professor of the Ministry of Education of Taiwan, in 2016. He also served as the Chairperson for the Electrical Engineering Department, from 1994 to 1997, the Vice President for research affairs, from 2005 to 2007, and the Senior Vice President at NSYSU, from 2007 to 2012. He is currently the National Chair Professor of the Ministry of Education, a Distinguished Researcher of the Ministry of Science and Technology, and a Distinguished Chair Professor with NSYSU. He has authored more than 580 refereed journal articles and 300 conference papers and has personally supervised 57 graduated Ph.D. He holds over 300 patents, including 103 U.S. patents. He is the author of *Design of Nonplanar Microstrip Antennas and Transmission Lines* (Wiley, 1999), *Compact and Broadband Microstrip Antennas* (Wiley, 2002), and *Planar Antennas for Wireless Communications* (Wiley, 2003). His published articles have been cited over 33,700 times with an H-index of 87 in Google Scholar.

Dr. Wong served or currently serves as an IEEE AP-S AdCom Member, an IEEE Transactions on Antennas and Propagation Track Editor/Associate Editor, an IEEE Transactions on Antennas and Propagation Paper Awards Committee Member, and an AP-S Field Awards Committee Member. He received the Outstanding Research Award three times (1995, 2000, and 2002) from the Taiwan National Science Council. He also received the Outstanding Electrical Engineering Professor Award (2003) from the Institute of Electrical Engineers of Taiwan and the Outstanding Engineering Professor Award (2004) from the Institute of Engineers of Taiwan. In 2008, the research achievements on handheld device antennas of NSYSU Antenna Laboratory led by him was selected to be top 50 scientific achievements of Taiwan Ministry of Science and Technology in past 50 years (1959–2009). He was a recipient of the 2010 Outstanding Research Award of Pan Wen Yuan Foundation and selected as top 100 Honor of Taiwan by Global Views Monthly, in August 2010, for his contribution in mobile antenna researches. He was also a recipient of the Academic Award (2012) from the Taiwan Ministry of Education and the Outstanding Distinguished Researcher Award (2013) from the Taiwan Ministry of Science and Technology. He and his graduate students have been awarded the Best Paper Award (APMC Prize) from 2008 APMC and the Best Student Paper Award/Young Scientist Award from 2007 ISAP, 2008 APMC, 2009 ISAP, 2010 ISAP, 2012 ISAP, and 2016 ISAP. His graduate students also won the First Prize of 2007 and 2009 Taiwan National Mobile Handset Antenna Design Competition. He was awarded the Best Associate Editor two times (2015 and 2016) for the IEEE Transactions on Antennas and Propagation. He was also a PE7 Panel Member of 2015, 2017, and 2019 European Research Council Advanced Grant Panel and a Chief Consultant of the Institute of Antenna Engineers of Taiwan. He also served as the Chair for the Judge Panel (2014–2021) of the National Communication Antenna Design Competition organized by the Taiwan Ministry of Economics. He served as the General Chair for 2012 APMC, 2014 ISAP, and 2016 APCAP, Kaohsiung. He was elected as a Thomson Reuters Highly Cited Researcher in both 2014 and 2015 and also elected as an Elsevier Most Cited Researcher in 2015. In 2022, he was selected by Research.com to be ranked #99 in Full World Ranking and #1 in Full Taiwan Ranking in the 2022 Edition of Ranking of Top 1000 Scientists in the field of electronics and electrical engineering. He is a Thomson Reuters Highly Cited Researcher and an Elsevier Most Cited Researcher.

CHI-JUI HO (Student Member, IEEE) received the B.S. degree in electronic engineering from Chung Yuan Christian University, Taoyuan, Taiwan, in 2021. He is currently pursuing the M.S. degree with the National Sun Yat-sen University, Kaohsiung, Taiwan. His main research interests include mobile MIMO antennas, multi-port wideband patch antennas and MIMO access-point antennas for 5G/5G+ mobile communication applications.

WEI-YU LI (Member, IEEE) was born in Taipei, Taiwan, in 1981. He received the B.S. degree in electrical engineering from Feng Chia University, Taichung, Taiwan, in 2004, and the M.S. and Ph.D. degrees in electrical engineering from the National Sun Yat-sen University (NSYSU), Kaohsiung, Taiwan, in 2006 and 2009, respectively.

After graduated from NSYSU, in 2009, he has been with the Information and Communication Research Laboratories (ICL), Industrial Technology Research Institute (ITRI), Hsinchu, Taiwan, participating and leading advanced research for development of emerging wireless antenna technologies. From April 2012 to October 2012, he was an Exchange Guest Researcher with the National Institute of Information and Communications Technology (NICT), Tokyo, Japan. He is currently a Deputy Technology Manager at ITRI. He has authored or coauthored 30 refereed journal articles and 40 conference papers. He holds over 70 patents, including U.S., Taiwan, and EU patents. His published articles have been cited 1,380 times with an H-index of 22 in Google Scholar.

Dr. Li has been selected as an International Steering Committee Member of 2019–2021 ISAP. He also served as an AdCom Member of the Institute of Antenna Engineers of Taiwan (2014, 2015, and 2018–2022). He also served as a member of the Judge Panel (2014 to 2022) for the National Terminal Antenna Design Competition organized by the Taiwan Ministry of Economics. He received the Young Scientist Award from 2007 ISAP and the Best Paper Award (APMC Prize) from 2008 APMC. He has been a principal investigator or a co-principal investigator of many research projects in ITRI and has received numerous recognitions, including the First Prize of the Outstanding Research Award of ITRI, in 2010, the Solar Industrial Award (SIA) of Europe, in 2011, the Outstanding Innovation Award of ITRI, in 2013, the Second Prize of the Outstanding Research Award of ITRI, in 2014, the 2015 Research and Development 100 Award Finalist of the U.S., the Outstanding Innovation Award of ITRI, in 2017, the First Prize of the Outstanding Industrialization Award of ITRI, in 2017, the Second Prize of the Outstanding Industrialization Award of ITRI, in 2020, and the Third Prize of the Outstanding Industrialization Award of ITRI, in 2021. He also received the Outstanding Lecturer Award of ITRI, in 2013, and the International Paper Award of ICL of ITRI, in 2020. He was the Chair of IEEE AP-S Tainan Chapter (2021–2022).